energies

MDPI

Article

Thermodynamic Analysis and Working Fluid Selection of a Novel Cogeneration System Based on a Regenerative Organic Flash Cycle

Haojie Chen and Man-Hoe Kim *

School of Mechanical Engineering & IEDT, Kyungpook National University, Daegu 41566, Korea
* Correspondence: manhoe.kim@knu.ac.kr; Tel.: +82-53-950-5576

Abstract: Recently proposed organic flash cycles maintain lower irreversibility in the evaporator than traditional organic Rankine cycles. This study presented a novel combined heat and power system that was based on a regenerative organic flash cycle, in order to improve thermal efficiency. Parametric analyses for the proposed combined heat and power system were carried out, using six working fluids, and performed with heat source temperatures and heat sink temperatures that ranged from 130 °C to 170 °C, and from 20 °C to 40 °C, respectively. The results showed that the preferable working fluid was altered, with a change in the operating condition. Isopentane, R1234ze(Z), R1233zd(E), and R245fa performed better at a cooling water temperature of 20 °C. The system that used R245fa showed more promising performance when the heat source temperatures were set to 150 °C and 160 °C. R365mfc was determined to be the best working fluid at a heat source temperature of 150 °C, and at cooling water temperatures of 30–40 °C. Finally, the analyses evaluated the year-round system performance on the basis of monthly ambient and water temperatures in Daegu, Korea, as the system's parameters. Compared to the single regenerative organic flash cycle, the thermal efficiency of the novel system improved significantly, from 8.37 % to 32.80% in August, and to 74.34% in February.

Keywords: regenerative organic flash cycle; combined heat and power; waste heat recovery; working fluid; efficiency

check for updates

Citation: Chen, H.; Kim, M.-H. Thermodynamic Analysis and Working Fluid Selection of a Novel Cogeneration System Based on a Regenerative Organic Flash Cycle. *Energies* **2022**, *15*, 7843. https://doi.org/10.3390/en15217843

Academic Editor: Pavel A. Strizhak

Received: 14 September 2022
Accepted: 19 October 2022
Published: 23 October 2022

Publisher's Note: MDPI stays neutral with regard to jurisdictional claims in published maps and institutional affiliations.

Copyright: © 2022 by the authors. Licensee MDPI, Basel, Switzerland. This article is an open access article distributed under the terms and conditions of the Creative Commons Attribution (CC BY) license (https://creativecommons.org/licenses/by/4.0/).

1. Introduction

Global energy demand continues to grow, due to the depletion of fossil fuel resources, and with the risk of climate change. Greenhouse gases that are generated by the burning of fossil fuels pose a significant risk to the environment, and are a serious and unpredictable cause of global climate change. Addressing these global energy and environmental challenges requires improvements to energy efficiency in the industry [1,2]. Recently, researchers are focusing on power generation systems based on the organic Rankine cycle (ORC), organic flash cycle (OFC), and supercritical carbon dioxide Brayton cycle (SCBC) using solar energy, geothermal energy, waste heat, or biomass energy [3]. Khatoon et al. [4] investigated a 10 MWe recompression supercritical carbon dioxide Brayton cycle with an in-house cycle design point and off-design codes. Sung et al. [5] conducted a thermoeconomic analysis of a biogas-fueled gas turbine that was integrated with an organic Rankine cycle for power generation, using food and sewage sludge waste heat. Ahmadi et al. [6] reviewed many applications of organic Rankine cycles that were powered by geothermal energy, and provided the latest materials for more systematically surveying the geothermal organic Rankine cycle.

The ORC with low boiling point working fluid retains widespread application in energy recovery from industrial waste heat sources. Muhammad et al. [7] reported on an experimental investigation of a small-scale (1 kW range) organic Rankine cycle system for net electrical power output ability, which used low-grade waste heat from steam. They

found that the measured electrical power output and enthalpy determined power output (considering isentropic efficiency) differed by 40%. Moreover, the ORC configuration is simple, and results in lower investment and less maintenance compared to other complicated technologies. For the basic ORC, the best thermal efficiency does not mean the highest net output owing to the temperature mismatch in the isothermal evaporation process, which has a certain amount of thermal energy destruction. Advanced technologies, such as the SCBC and ORC [8], using zeotropic working fluid mixed with two or more compositions, trilateral flash cycle (TFC) [9], and an OFC [10] have been exploited to strengthen the performance of power generation systems. An SCBC that uses carbon dioxide as a working fluid needs a pressure bigger than the critical pressure of carbon dioxide to attain the demand of temperature by avoiding isothermal evaporation [11]. Therefore, an SCBC uses a compressor to bring carbon dioxide to a high pressure, increasing the energy consumption of compression, investment cost, and development risk [12]. Thus, to improve the temperature balance during isothermal evaporation processes, Li et al. [13] examined an ORC system's performance using zeotropic working fluids based on different parameters. The thermal efficiency was increased with decreased irreversibility in the evaporator, using a smaller mean temperature difference. However, the area of the evaporator needs to be large in order to overcome the low conductivity disadvantage of the zeotropic. Thus, an ORC with mixed working fluids is less cost effective than one with pure working fluids. Smith et al. [14] introduced the TFC, which reduced the irreversibility under isothermal evaporation processes. From the perspective of reducing exergy damage, this is a promising solution; however, so far, the two-phase expansion process has made it challenging for researchers to find a suitable and effective two-phase expander [15]. The OFC is an appropriate solution for the large exergy loss during the heat exchange process in ORC evaporators.

With an updated TFC, the OFC inherits the advantages of TFC, such as simplicity, safety, and low irreversibility in the evaporator. In addition, compared with a TFC using a two-phase expander, the combination of the flash chamber, throttle valve, and the traditional expander is critical to improving construction flexibility. However, reducing exergy damage at the cost of increasing throttling losses prompted researchers to seek suitable solutions by improving the OFC's configuration and layout. As a result of high-temperature matching and improved efficiency, many researchers have studied OFCs with improved structures [16,17]. Lee et al. [18] compared a basic organic flash cycle (BOFC), an organic flash cycle with a two-phase expander (OFCT), and an ORC. The results show that the OFC is superior when using a low-temperature heat source for heating the working fluid. Based on the improved structure, Wang et al. [19] conducted a comprehensive analysis of four OFC systems. The organic flash Rankine cycle II retained a maximum thermal efficiency of 8.99%, while the BOFC, ROFC, and the organic flash Rankine cycle I only achieved 6.17%, 8.37%, and 7.74 %, respectively. Meng et al. [20] analyzed the performance of regenerative OFC (ROFC) systems, which included an OFC with an internal heat exchanger (IHE), an OFC with a regenerator, an ROFC with IHE, and a modified OFC (MOFC). The results showed that the net power output of the MOFC was higher than that of the BOFC. The MOFC's net production increased by 66.2% under the heating of geothermal water at 120 °C. The MOFC needed 42% less condenser area compared to the BOFC, whereas 51–78% more evaporator area is required to increase the heat transfer performance under smaller temperature difference conditions. Chen et al. [21] studied an OFC using one ejector or more, according to thermodynamic analysis. Compared with the traditional ORC, the performance of the OFC (SESF-OFC) and BOFC based on a single ejector and single flash evaporator was not as good as the ORC's, owing to its lower overall exergy efficiency. The overall efficiency of the OFC-based single ejector and dual flash evaporator (SEDF-OFC), and OFC-based dual ejector and dual flash evaporator (DEDF-OFC), increased by 10.37% and 15.01%, respectively.

In order to enhance the versatility of a single power generation system, several recent studies and analyses have been carried out regarding the combination of basic power generation and refrigeration cycles. Subha Mondal et al. [22] proposed an OFC-based cooling and power cycle, which also used an ejector. Nevertheless, in the combined cooling and power cycle, the ejector was placed differently as compared to the SESF-OFC that was introduced by Chen et al. [21]. The ejector was placed at the liquid outlet of the separator, in order to absorb the primary liquid in the flash cycle, and the second vapor stream that was generated by the refrigeration cycle evaporator. A cooler was built to absorb the heat of the working fluid that was discharged from the turbine and ejector. Then, the condensed liquid entered the refrigeration cycle via the throttle valve, and the power generation cycle via the pump. Van et al. [23] found that the exergy efficiency of power generation systems for district heating is always higher than that of power plants for pure power generation. Recently, researchers have not only combined refrigeration for the basic power generation cycle, but also conducted effective design and comprehensive analyses of the combined heat and power (CHP) system. It has great potential to improve the overall performance of various systems [24].

Gaoliang et al. [25] studied ORC-combined cooling, heating, and power (CCHP) systems that were heated by waste heat. Moreover, by analyzing the thermal efficiency and performance coefficient, a comparative study of the single-fluid and two-fluid CCHP systems was conducted. The results showed that applying superheat to the inlet of the turbine can reduce the systems' irreversibility. The analytic hierarchy process optimized the working fluids. R1234ze (E) and heptane/R601a outperformed the selected different working fluids for the two CCHP systems. Wang et al. [26] introduced an ORC-based CHP system in which biomass fuel was used for the heat supply, and the designed system simultaneously achieved 1.66 kW of net power output and 37.16 kW of thermal energy. Furthermore, exergy analysis showed that post-heating caused the greatest irreversibility, significantly reducing exergy efficiency. Arabkoohsar et al. [27] studied and improved a CHP-ORC plant for waste heat recovery, in order to increase the net power output share in total energy output. The results demonstrated that the electrical, thermal, and exergy efficiencies of the transformed CHP-ORC power plant increased by 20%, 10%, and 9%, respectively, compared with the old design. The above-mentioned CHP system was mainly based on the ORC cycle. Rostamzadeh et al. [28] analyzed a CCHP system that was based on the Kalina cycle (KC), using a comparative study with the ORC-CHP system. The best thermal efficiency of the CCHP system on the basis of the ORC and KC reached 76.54% and 77.32%, respectively, and the best exergy efficiency of the CCHP system on the basis of the ORC and KC reached 48.37% and 31.2%, respectively. Many studies on the effects of working fluids (pure and mixtures) in ORC systems have been conducted [29,30]; moreover, eco-friendliness, such as low-GWP and safety (toxicity and flammability) issues, have attracted researchers [31]. Aghahosseini and Dincer [29] conducted thermodynamic analysis of a low-grade heat source ORC, and analyzed cycle performance using several different pure (R123, R245fa, R600a, R134a) and zeotropic-mixture (R407C, R404A) working fluids. Tabrizi and Bonalumi [30] performed a techno-economic performance analysis of an ORC using a 2-propanol/1-butanol zeotropic mixture and 2-propanol/water azeotropic mixture as a working fluid. Scharrer et al. [32] modelled the Carnot battery system, using a pilot plant as a reversible heat pump (20 kW)/organic Rankine cycle (7–13 kW) system coupled with a sensible hot water storage system. They used the operational data from local energy suppliers to verify the heat storage components of the simulation model, while thermal machines were based on simulation and experimental data from the pilot plant. Many experimental studies for industrial applications of the ORC have been carried out [33–35].

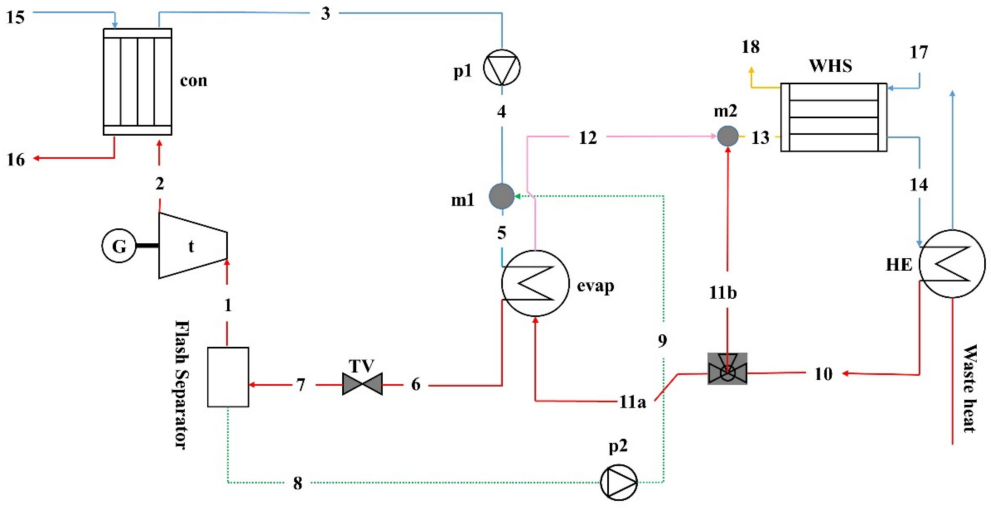
Several researchers have focused on the OFC to reduce irreversibility in the evaporator; however, the problem was that the thermal efficiency was lower than in the ORC. Therefore, this study was inspired by the ORC-CHP system, and investigated the ROFC-based CHP system to improve thermal use efficiency. Six suitable working fluids were selected as

medium-low heat sources, in order to explore whether there are more suitable working fluids than isopentane, which has been widely investigated by many researchers. Furthermore, the effects of heat source and cooling water temperatures on the ROFC's performance for six working fluids were comprehensively analyzed, considering that different working fluids perform best under varying specific working conditions. Finally, based on the monthly ambient and water temperatures in Daegu, South Korea, the ROFC-based cogeneration system was analyzed. The demand for hot water varies with monthly environmental and water temperatures, which leads to changes in the required amounts of electricity and heat power each month during the year.

2. Methodology

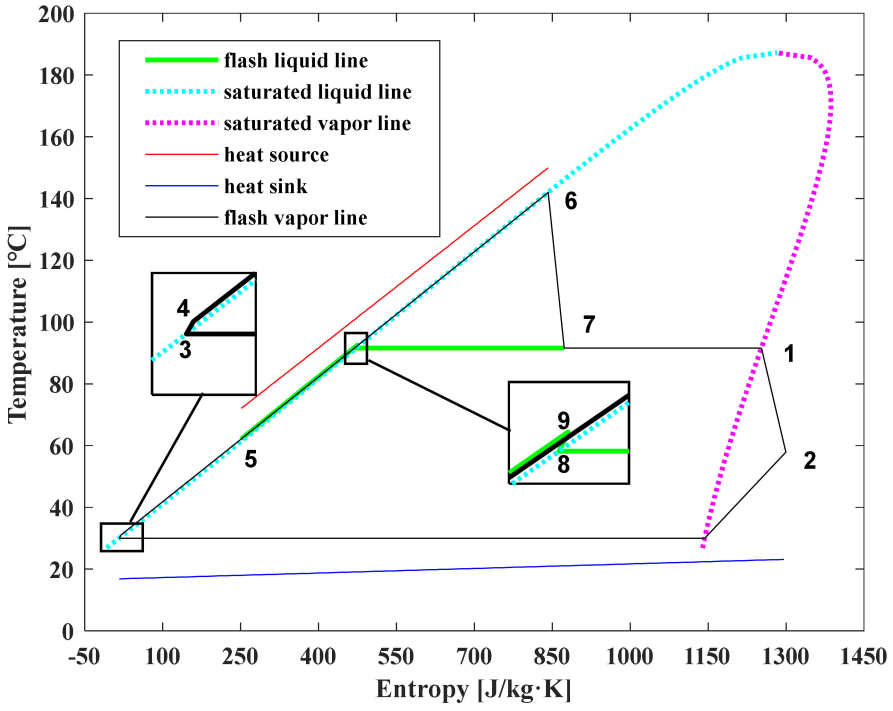
2.1. System Description

Figure 1 presents a schematic layout of the ROFC-based CHP system applied for recovering waste heat. Waste heat at 130 °C–170 °C provides thermal energy for heating water via the heat exchanger (HE). Heated water is precisely divided into two streams for the water heating system (WHS), based on the heat demand (heat transfer rate in WHS) calculated using the monthly ambient and water temperature in Daegu, Korea, for basic conditions shown Table 1 [36]. One stream passes through the evaporator, and the other stream passes through mixer2 (m2), where it is mixed with heating water from the evaporator outlet. The mixed heated water heats the water in the WHS, changing the water temperature in different months (Table 1) up to 45 °C for a household WHS, then passes through the HE to finish the cycle. For the power generation cycle, the working fluid isobarically absorbs heat energy from heated water, and flows through the throttling valve to expand from a saturated fluid into a two-phase mixture. The two-phase fluid is distributed into a vapor that is ducted into the turbine to generate electricity, and liquid that is introduced to pump2 (p2) is pumped up to evaporation pressure for regeneration. The vapor at high temperature and low pressure from the turbine passes through the condenser to complete a phase change into liquid, employing heat rejection. The liquid phase of the working fluid is pumped into mixer1 (m1), in which vapor from the outlet of pump1 (p1) is mixed with saturated liquid at a higher temperature for regeneration, and the mixed liquid is finally transmitted to the evaporator to make the process cyclic.



(**a**)

Figure 1. *Cont.*



(**b**)

Figure 1. Schematic diagram of the ROFC-based CHP system: (**a**) system layout; (**b**) temperature–entropy diagram.

Table 1. Parameters of monthly temperature and heat demand in Daegu, South Korea.

Month	Ambient Temperature (°C)			Median Water Temperature (°C)	Water Flow Rate in WHS (kg/s)	Heat Transfer Rate in WHS (kW)
	Max.	Min.	Avg.			
January	5.00	−3.00	1.00	13.50	8.50	1124.55
February	7.50	−2.00	2.75	12.50	8.50	1160.25
March	13.00	3.50	8.25	12.25	6.00	825.30
April	19.00	9.50	14.25	14.00	5.80	755.16
May	24.00	14.50	19.25	16.50	5.50	658.35
June	27.00	19.00	23.00	19.50	5.30	567.63
July	29.50	22.50	26.00	23.00	4.80	443.52
August	29.50	22.50	26.00	25.50	4.50	368.55
September	26.00	18.00	22.00	24.00	6.00	529.20
October	21.00	11.50	16.25	21.00	6.50	655.20
November	13.50	5.00	9.25	18.00	7.00	793.80
December	7.50	−1.00	3.25	15.50	8.50	1053.15

2.2. Energy Analysis

In order to avoid the complexity of the CHP system's simulation, the following assumptions were made [37,38]:

(1) Pressure drops during every process were considered zero.
(2) This cycling process was a steady flow process.
(3) Heat losses from the components were negligible.
(4) The kinetic and potential energies were to be zero.
(5) The working fluids flowed into the pumps in the saturated state.
(6) The efficiencies of pumps, turbines, and generators were unchanged.

The energy balance equations for each component were described as follows.

For m1, the specific enthalpy h_5 was calculated using Equation (1):

$$h_5 = (1 - x_7)h_9 + x_7 h_4 \tag{1}$$

The working fluid was heated via the evaporator. The rate of heat input could be calculated as follows:

$$\dot{Q}_{in,ROFC} = \dot{m}_{11a}(h_{11a} - h_{12}) \tag{2}$$

The mass flow rates at the inlet and outlet of the evaporator were determined, respectively, as follows:

$$\dot{m}_5 = \dot{Q}_{in,ROFC}/(h_6 - h_5) \tag{3}$$

$$\dot{m}_6 = \dot{m}_5 \tag{4}$$

The mass flow rate at the inlet of the turbine was given by the following:

$$\dot{m}_1 = x_7 \dot{m}_6 \tag{5}$$

The mass flow rate at the inlet of the p2 was determined as follows:

$$\dot{m}_8 = (1 - x_7)\dot{m}_6 \tag{6}$$

The rate of power generated in the turbine was calculated as follows:

$$\dot{W}_t = \dot{m}_1(h_1 - h_2) \tag{7}$$

The mass flow rate at the inlet of the condenser and the rate of heat rejected were described, respectively, as follows:

$$\dot{m}_2 = \dot{m}_1 \tag{8}$$

$$\dot{Q}_{out} = \dot{m}_2(h_2 - h_3) \tag{9}$$

The mass flow rates at the inlet and outlet of p1 were, respectively, as follows:

$$\dot{m}_3 = \dot{m}_2 \tag{10}$$

$$\dot{m}_4 = \dot{m}_3 \tag{11}$$

The rates of work assumption in p1 and p2 were determined, respectively, as follows:

$$\dot{W}_{p1} = \dot{m}_3(h_4 - h_3) \tag{12}$$

$$\dot{W}_{p2} = \dot{m}_8(h_9 - h_8) \tag{13}$$

The specific enthalpy of h_{13} was calculated using Equation (14):

$$h_{13} = \dot{m}_{17} C_p \left(\frac{T_{18} - T_{17}}{\dot{m}_{13}} \right) + h_{14} \tag{14}$$

where C_p was assumed to be the specific heat of water at standard temperature and pressure, in order to simplify the calculation of heat demand from the WHS. $\dot{m}_{17}$ is the mass flow rate of hot water that provided heat to households. We analyzed the ambient and water temperatures for each month, in order to calculate the split of $\dot{m}_{10}$.

If $h_{13} > h_{12}$, the $\dot{m}_{11b}$ was determined through an energy balance in m2 as follows:

$$\dot{m}_{11b} = \dot{m}_{10}(h_{13} - h_{12})/(h_{10} - h_{12}) \tag{15}$$

If $h_{13} < h_{12}$

$$\dot{m}_{11b} = 0 \tag{16}$$

The rate of heat required in the WHS was given as shown below:

$$\dot{Q}_{WHS} = \dot{m}_{13}(h_{13} - h_{14}) \tag{17}$$

The network output of the CHP system based on the ROFC was determined as shown below:

$$\dot{W}_{net} = (\dot{W}_t - \dot{W}_{p1} - \dot{W}_{p2})\eta_g \tag{18}$$

The thermal efficiency of the ROFC was computed as follows:

$$\eta_{th,ROFC} = \dot{W}_{net}/\dot{Q}_{in,ROFC} \tag{19}$$

The thermal efficiency of the ROFC-based CHP system was computed as follows:

$$\eta_{th,CHP} = (\dot{W}_{net} + \dot{Q}_{WHS})/\dot{Q}_{in,CHP} \tag{20}$$

where $\dot{Q}_{in,CHP}$ was described, as shown below:

$$\dot{Q}_{in,CHP} = \dot{m}_{10}(h_{10} - h_{14}) \tag{21}$$

The global thermal efficiency of the ROFC was described with the following:

$$\eta_{th,gl,ROFC} = \dot{W}_{net}/\dot{Q}_{in,gl,ROFC} \tag{22}$$

where $\dot{Q}_{in,gl}$ was calculated, as shown below:

$$\dot{Q}_{in,gl,ROFC} = \dot{m}_{11a}(h_{11a} - h_0) \tag{23}$$

Here, h_0 was assumed to be the specific enthalpy at a dead state.

The mass flow rate of cooling water was determined as follows:

$$\dot{m}_{16} = \dot{m}_{15} = \dot{Q}_{out}/(h_{16} - h_{15}) \tag{24}$$

2.3. Exergy Analysis

Exergy is defined to be the largest useful work that can be generated from the power generation cycle while it maintains balance with its surroundings at a given dead state. Exergy efficiency and destruction are vital indicators for analyzing the CHP system's performance because these can demonstrate the irreversibility of each component and the ability of power generation, which can offset the drawback of not revealing the system's weakness of single energy analysis.

Specific exergy flow at every state during calculation was determined as shown below:

$$e = h - h_0 - T_0(s - s_0) \tag{25}$$

Using the conservation rules of exergy for each component, the exergy destruction was calculated as follows:

For the evaporator, condenser, and the WHS, respectively, were determined as follows:

$$\dot{I}_{evap} = \dot{m}_{11a}(e_{11a} - e_{12}) - \dot{m}_5(e_6 - e_5) \tag{26}$$

$$\dot{I}_{con} = \dot{m}_2(e_2 - e_3) - \dot{m}_{15}(e_{16} - e_{15}) \tag{27}$$

$$\dot{I}_{WHS} = \dot{m}_{13}(e_{13} - e_{14}) - \dot{m}_{17}(e_{18} - e_{17}) \tag{28}$$

For pumps and the turbine, respectively, exergy destructions were determined as shown below:

$$\dot{I}_{p1} = \dot{m}_3 T_0 (s_4 - s_3) \tag{29}$$

$$\dot{I}_{p2} = \dot{m}_8 T_0 (s_9 - s_8) \tag{30}$$

$$\dot{I}_t = \dot{m}_1 T_0 (s_2 - s_1) \tag{31}$$

For the throttling valve, the exergy destruction was determined as follows:

$$\dot{I}_{TV} = \dot{m}_6 (e_7 - e_6) \tag{32}$$

For mixers, exergy destructions were calculated as follows:

$$\dot{I}_{m1} = \dot{m}_4 e_4 + \dot{m}_9 e_9 - \dot{m}_5 e_5 \tag{33}$$

$$\dot{I}_{m2} = \dot{m}_{12} e_{12} + \dot{m}_{11b} e_{11b} - \dot{m}_{13} e_{13} \tag{34}$$

For the generator, the exergy destruction was given by the following:

$$\dot{I}_g = (\dot{W}_t - \dot{W}_{p1} - \dot{W}_{p2}) - \dot{W}_{net} \tag{35}$$

The total exergy destruction of the CHP system was calculated as follows:

$$\dot{I}_{total} = \dot{I}_{evap} + \dot{I}_{con} + \dot{I}_{WHS} + \dot{I}_{p1} + \dot{I}_{p2} + \dot{I}_t + \dot{I}_{TV} + \dot{I}_{m1} + \dot{I}_{m2} \tag{36}$$

The exergy input of the CHP system from the heat source was determined as follows:

$$\dot{E}_{in,CHP} = \dot{m}_{10} (e_{10} - e_{14}) \tag{37}$$

The global exergy input of the CHP system from the heat source was calculated as follows:

$$\dot{E}_{in,gl,CHP} = \dot{m}_{10} (e_{10} - e_0) \tag{38}$$

The exergy input of the ROFC from the heat source was determined with the following:

$$\dot{E}_{in,ROFC} = \dot{m}_{11b} (e_{11b} - e_{12}) \tag{39}$$

The global exergy input of the ROFC from the heat source was given by the following:

$$\dot{E}_{in,gl,ROFC} = \dot{m}_{11b} (e_{11b} - e_0) \tag{40}$$

The exergy efficiency of the ROFC was determined with the following:

$$\eta_{ex,ROFC} = \dot{W}_{net} / \dot{E}_{in,OFC} \tag{41}$$

The global exergy efficiency of the ROFC was described as follows:

$$\eta_{ex,gl,ROFC} = \dot{W}_{net} / \dot{E}_{in,gl,OFC} \tag{42}$$

The exergy efficiency of the CHP system was represented by the following:

$$\eta_{ex,CHP} = \left(\dot{W}_{net} + \dot{m}_{17} (e_{18} - e_{17}) \right) / \dot{E}_{in,CHP}. \tag{43}$$

The global exergy efficiency of the CHP system was determined with the following:

$$\eta_{ex,gl,CHP} = \left(\dot{W}_{net} + \dot{m}_{17} (e_{18} - e_{17}) \right) / \dot{E}_{in,gl,CHP} \tag{44}$$

2.4. Model Validation and Working Fluid Selection

The ROFC is combined with a WHS in which the heat demand varies with ambient and water temperatures. Therefore, the choice of working fluids should be selected considering both the ROFC and WHS. Indicators such as environment-friendly potential, thermal efficiency, exergy efficiency, and economical potential are critical in selecting the working fluids for optimal performance of the ROFC-based system [39]. According to existing literature, most working fluids cannot fulfill all these indicators. Each working fluid has its advantages in a specific set of conditions. In order to prevent the world from the polluted environment, related organizations advocate that low global warming potential (GWP) and ozone depletion potential (ODP) of working fluids should replace the high ones. Finally, cyclopentane, R1234ze(Z), R365mfc, isopentane, R1233zd(E), and R245fa are selected as the candidates taking into consideration the above-mentioned criteria. Table 2 then presents the properties of the six working fluids; all are dry fluids with advantages such as the high potential of power generation and less erosion for turbines compared to wet ones. For the WHS, water was used as the heat transfer fluid to meet the household heat demand that varies every month, which requires easy access for obtaining water whenever and whatever amount the WHS needs. More importantly, the properties of water and selected working fluids are easy to be obtained using REFPROP [40] from which the first part of the optimization process can be finally completed.

Table 2. Properties of six working fluids selected for the ROFC [41–43].

Working Fluids	Chemical Formula	Molar Mass (g/mol)	Critical Pressure (kPa)	Critical Temperature (°C)	ODP/GWP	Safety Group
Cyclopentane	C_5H_{10}	70.13	4583	238.6	0/11	A3
R1234ze(Z)	$C_3H_2F_4$	114.00	3530	150.1	0/6	A2L
R365mfc	$C_4H_5F_5$	148.07	3266	186.9	0/804	-
Isopentane	C_5H_{12}	72.15	3378	187.2	0/11	A3
R1233zd(E)	$C_3ClH_2F_3$	130.50	3570	165.6	0/1	A1
R245fa	$C_3H_3F_5$	134.05	3651	153.9	0/858	B1

Figure 2 is a flowchart from which we obtained the maximum net work (W_{net}) and global exergy efficiency, using MATLAB and corresponding properties, such as flash pressure and condensation temperature. In order to evaluate the optimal working fluid for the ROFC, it was assumed that $Q_{WHS} = 0$ to simplify the process. Here, MATLAB provided access to obtain the properties of these working fluids by linking REFPROP, using a specified code. Then, the simulation could be conducted in the ideal environment, based on MATLAB. The temperature of the heat source was given as 150 °C, and the minimum temperature difference between the working fluid and heating water was set at 8 °C. In order to interpret the flowchart in detail, Table 3 presents the other basic properties used for optimization. The condenser outlet temperature was assumed to be at least 10 °C higher than T_{15}. The flash pressure in the range of (P_1, P_2) was divided into 100 units, with equal pressure intervals to determine the optimal flash pressure for the maximum corresponding global exergy efficiency.

The obtained results at the heat source temperature of 130–150 °C were compared with those computed by Wang et al. [19], and the maximum differences between the present study and Wang et al. [19] for the net work and exergy efficiency were 2.5 and 1.3%, respectively. Table 4 shows the detailed optimization results.

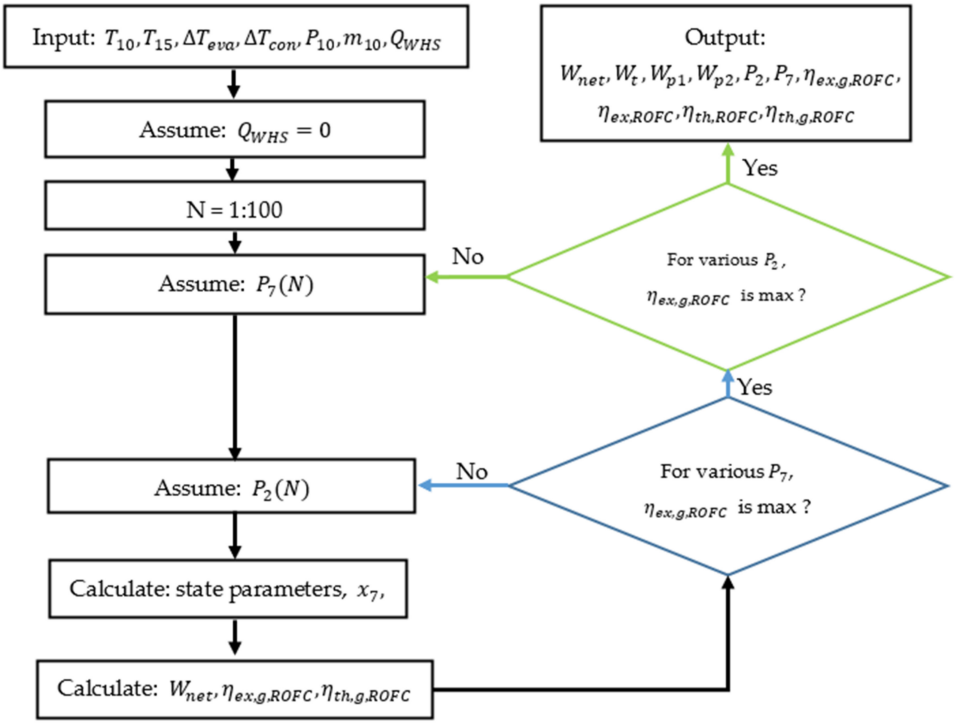


Figure 2. Parametric optimization for the ROFC.

Table 3. Basic given conditions used for optimization [19].

Parameters (Unit)	Given Conditions
Pressure of the hot water (kPa)	1000
Heat transfer fluid (HTF)	Water
Inlet temperature of the HTF (°C)	150
Mass flow rate of the HTF (kg/s)	5
OFC working fluid	Isopentane
Minimum temperature difference at condenser (°C)	10
Minimum temperature difference at evaporator (°C)	8
Ambient temperature (°C)	20
Condensation temperature (°C)	30
Efficiency of the generator (%)	90
Efficiency of the turbine (%)	75
Efficiency of the pump (%)	70

Table 4. Thermodynamic parameters of the optimized ROFC system.

State Point	Working Fluid	T [°C]	P [kPa]	h [kJ/kg]	s [kJ/(kg·K)]	$\dot{m}$ [kg/s]
1	Isopentane	91.6	600	1.25	442.59	3.92
2	Isopentane	57.9	109	1.30	396.23	3.92
3	Isopentane	30.0	109	0.02	5.00	3.92
4	Isopentane	31.02	1628	0.02	8.55	3.92
5	Isopentane	62.1	1628	0.25	82.56	7.63
6	Isopentane	142.0	1628	0.84	304.24	7.63
7	Isopentane	91.6	600	0.87	304.24	7.63
8	Isopentane	91.6	600	0.47	158.05	3.71
9	Isopentane	92.5	1628	0.47	160.77	3.71
10	Water	150.0	1000	1.84	632.50	5.00
11a	Water	150.0	1000	1.84	632.50	0.00
11b	Water	150.0	1000	1.84	632.50	5.00
12	Water	70.1	1000	0.96	294.20	5.00
13	Water	70.1	1000	0.96	294.20	5.00
14	Water	70.1	1000	0.96	294.20	5.00
15	Water	18.0	101	0.27	75.64	18.16
16	Water	23.2	101	0.34	97.18	18.16

3. Results and Discussion

This section analyzes several parameters that influence the performance of the CHP system.

3.1. The Effect of Flash Pressure on ROFC Performance

Figure 3 shows saturation vapor pressure curves for the six selected working fluids. Figure 4 shows the net powers as a function of the flash pressure for R245fa, R1234ze(Z), isopentane, R1233zd(E), R365mfc, and cyclopentane. For all working fluids that were considered in the study, the effect of the flash pressure on the net work showed the same trend. The net work increased with the flash pressure, reached a maximum at a certain pressure, and then decreased again. An optimal flash pressure exists where the maximum net power output appears, resulting from a change in the mass flow rate and enthalpy drop during the expansion process of the ROFC (the enthalpy drop increases with an increase in the flash pressure, but the mass flow rate weakens because the quality of the working fluid weakens). Furthermore, R245fa is appropriate if only the net power output is considered, since the maximum net power output is on the curve of R245fa.

Figure 5 illustrates the influence of flash pressure on the global exergy efficiencies for several working fluids. The changing trend of global exergy efficiency was not considerably different from the variation trend of net power output. The exergy input was always the same because exergy input was calculated using a dead state. Figure 6 demonstrates the effect of flash pressure on the exergy efficiencies for six working fluids. Using isopentane maximized the global exergy efficiency, followed by R1234ze(Z), R1233zd(E), R245fa, cyclopentane, and R365mfc. The exergy efficiency initially increased because of the reduction in exergy input, but decreased a little or approximately became balanced because the decrease rate of the net power output tended to balance the decrease rate of the exergy input.

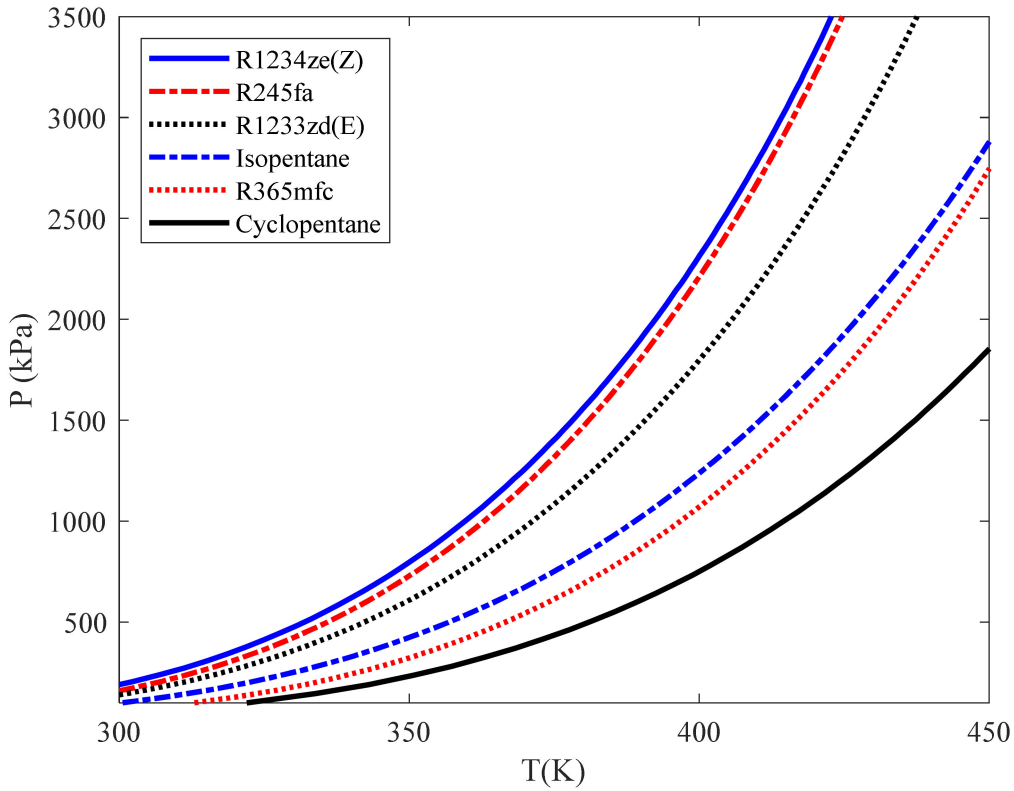


Figure 3. Saturation vapor pressure–temperature(P–T) diagram.

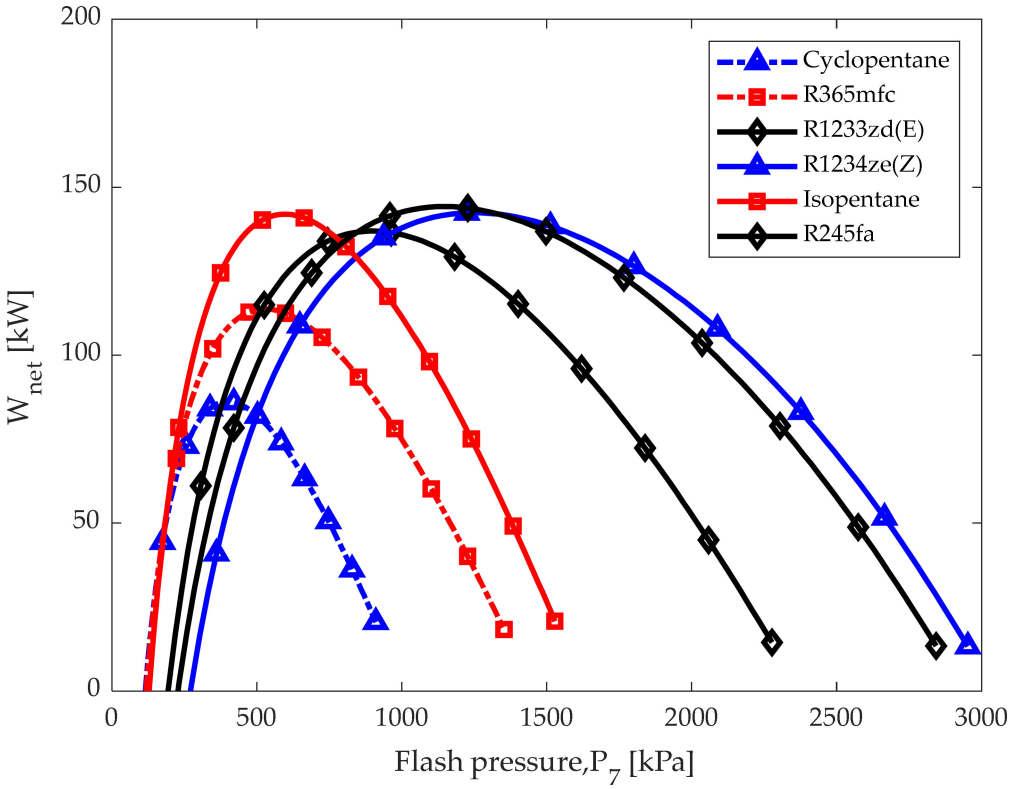


Figure 4. Effect of flash pressure on the net power outputs.

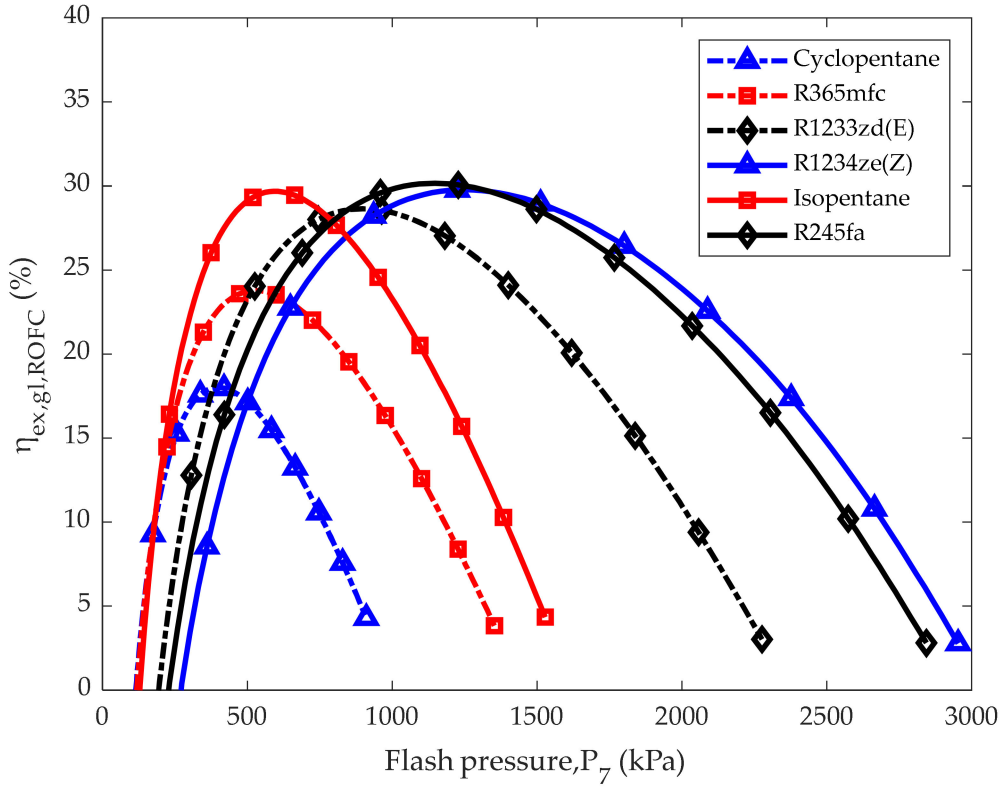


Figure 5. Effect of flash pressure on the global exergy efficiencies.

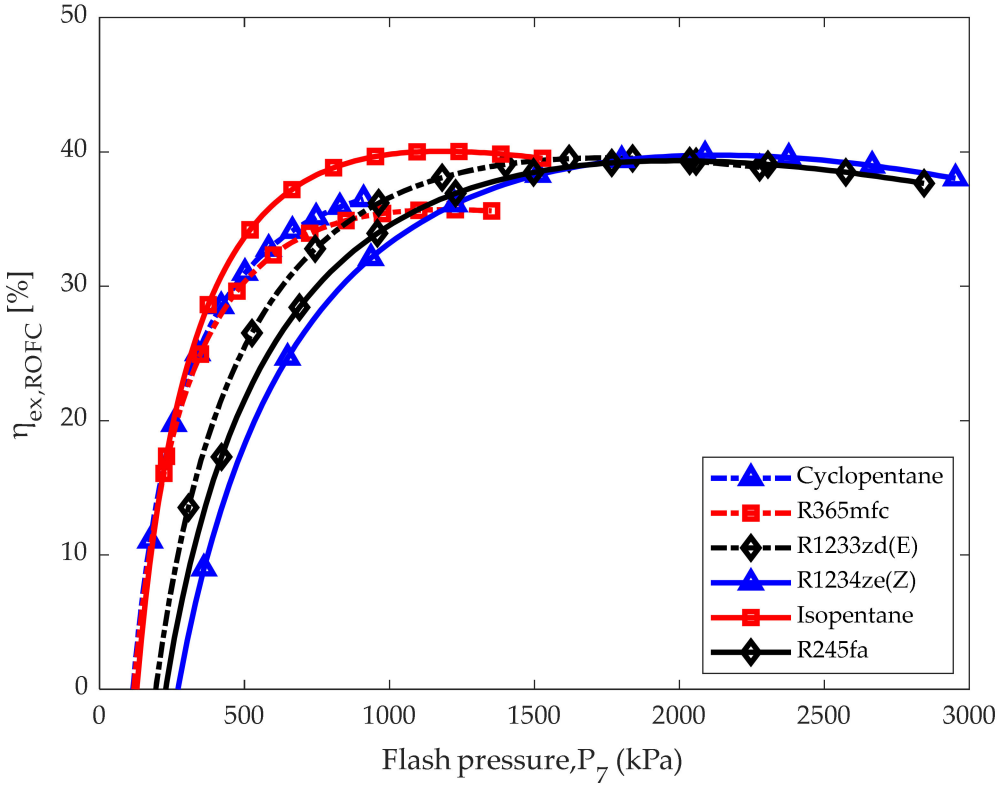


Figure 6. Effect of flash pressure on the exergy efficiencies.

In Figure 7, the effect of flash pressure on the global thermal efficiencies for six working fluids was similar to that in Figure 5, because the energy input was fixed, even though the flash pressure changed. The net power output initially increased when the pressure drop in the turbine increased, then decreased when the mass flow rate in the turbine decreased, because the quality of the working fluid in the flash separator decreased. Interestingly, R245fa with a large flash pressure range performed better than other working fluids. Isopentane also showed a relatively higher global thermal efficiency, followed by R1234zd(E), R1233zd(E), R365mfc, and cyclopentane. Figure 8 presents the effect of flash pressure on the thermal efficiencies of six working fluids. All of the fluids showed that the thermal efficiency initially increased rapidly, and then increased slightly because of the simultaneous increase in the net power output and the decrease in the heat input as the flash pressure increased. Isopentane showed the highest thermal efficiency for the ROFC, and R1233zd(E) and R1234ze(Z) also performed relatively efficiently compared with the other three working fluids.

3.2. The Optimal Working Fluid for ROFC

Working fluid selection is essential for improving the performance of a power generation system. Therefore, the working fluids suitable for the heat source at medium-low temperatures were studied, in order to determine the optimal working fluid. Table 5 shows that an ROFC with R245fa as a working fluid is proper, as a result of its maximum global exergy efficiency. However, it does not mean that R245fa is the most suitable working fluid for an ROFC, since of the largest operating pressure for which the quality of tube and components must be higher than that for other working fluids under lower operating pressures. The quality has a linear relationship with the price. Thus, isopentane is an appropriate option to obtain significant net power output, and costs less for an ROFC.

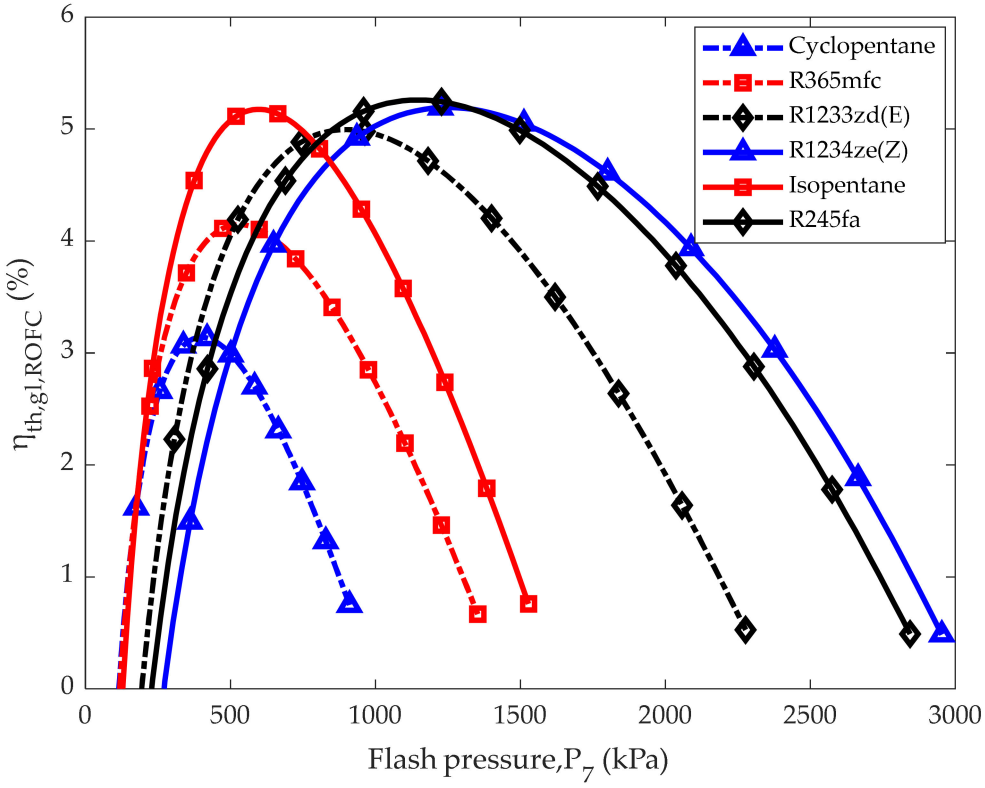


Figure 7. Effect of flash pressure on the global thermal efficiencies.

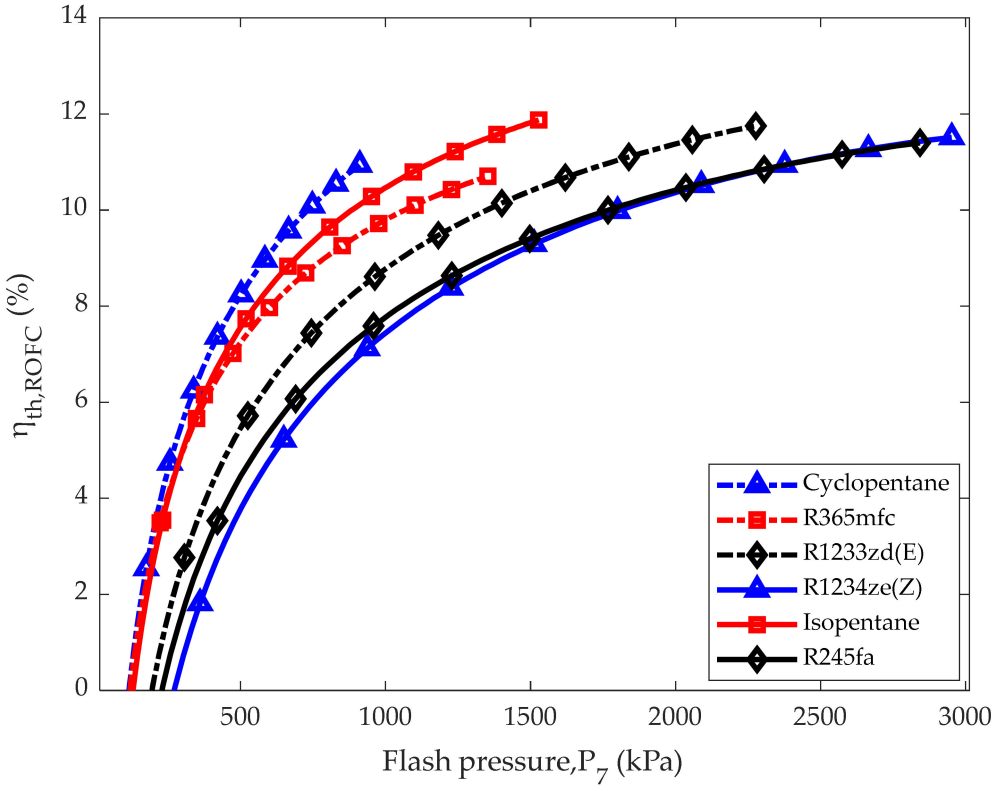


Figure 8. Effect of flash pressure on the thermal efficiencies.

Table 5. Optimized global exergy efficiency and corresponding parameters for an ROFC with a heat source of 150 °C, and a cooling water temperature of 20 °C.

Working Fluids	Evaporation Pressure (kPa)	Flash Pressure (kPa)	Condensation Pressure (kPa)	Net Power Output (kW)	Global Exergy Efficiency (%)
Cyclopentane	973.01	395.60	101.33	86.11	18.01
R365mfc	1452.90	531.10	101.33	113.72	23.78
R1233zd(E)	2376.60	897.60	154.00	136.99	28.64
Isopentane	1628.07	600.00	109.17	141.97	29.68
R1234ze(Z)	3052.90	1253.00	209.00	142.41	29.78
R245fa	2943.60	1148.60	178.08	144.00	30.16

3.3. The Effect of Heat Source Temperature on ROFC Performance

In an ideal Rankine cycle, its performance can be enhanced by increasing the evaporation temperature and decreasing the condensation temperature as much as possible; therefore, these two parameters should be the key variables for studying the performance of an ROFC for selected working fluids. In order to analyze the effect of heat source temperature on the ROFC's performance, isopentane was chosen as the working fluid, and the heat source temperature was set at 130 °C, 140 °C, 150 °C, 160 °C, and 170 °C. The heat sink temperature was set at a constant 20 °C. Other basic parameters are given in Table 3.

Figure 9 presents the effect of heat source temperature on net power output. There is no net power output presented for R245fa and R1234ze(Z), when the heat source temperature is $\geq$ 170 °C and $\geq$ 160 °C, respectively, since the evaporation temperature should not be higher than a fluid's critical temperature. It can be found from the figure that for each working fluid, the net power output increased as the heat source temperature increased. Moreover, the maximum net power output was achieved using isopentane as the working fluid, followed by R245fa, R1233zd(E), R1234ze(Z), R365mfc, and cyclopentane at 130 °C. For a heat source temperature $\geq$ 150 °C, R245fa showed the highest net power output. Although R245fa performed similarly at heat source temperatures of 140 °C and 150 °C, the ROFC with isopentane as the working fluid generated 172 kW of net power, which was 20 kW less than 192 kW that was produced by the ROFC using R245fa as the working fluid at 160 °C.

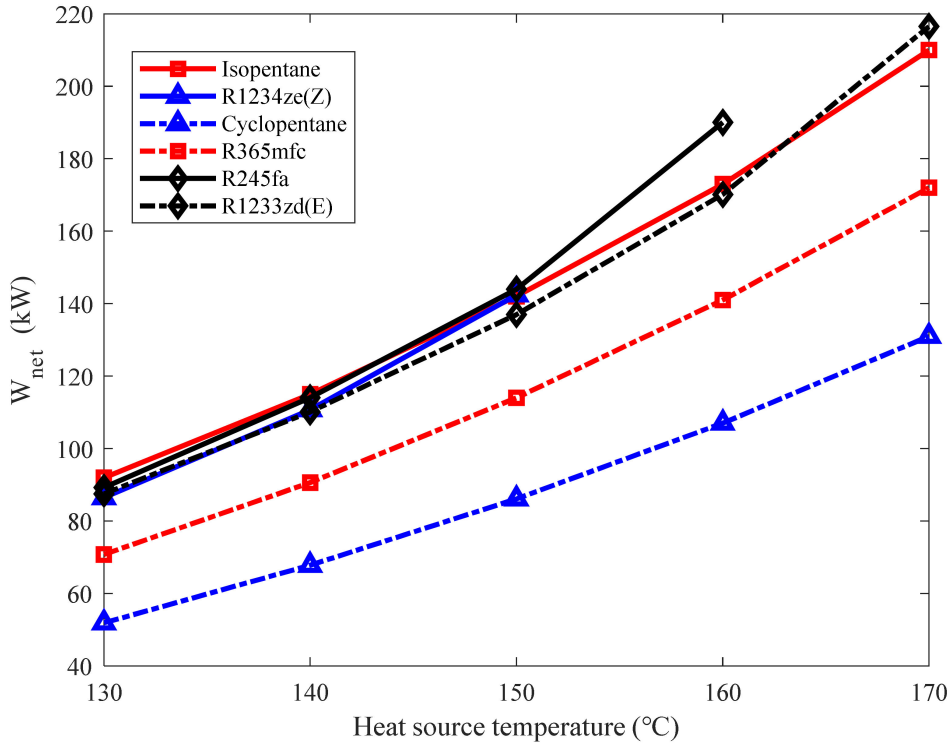


Figure 9. Effect of heat source temperature on the net power output.

Figure 10 demonstrates the influence of the heat source temperature on global exergy efficiency. Considering the global exergy efficiency at the heat source temperature of 130 °C, the six studied working fluids could be divided into two groups, according to their performance. The working fluids R245fa, isopentane, R1234ze(Z), and R1233zd(E) performed better than the other fluids, with global exergy efficiencies greater than 25%. The ROFC with R365mfc yielded 20% global exergy efficiency, and only around 15% global exergy efficiency was obtained when cyclopentane was used as the working fluid. The global exergy efficiency improvement of 10%, when using the working fluids from the best group, indicates that they are superior to cyclopentane. The figure also indicates that the global exergy efficiency increased for each working fluid as the heat source temperature increased. Moreover, as 10 °C increased, around a 2.5% enhancement in global exergy efficiency was obtained for each working fluid.

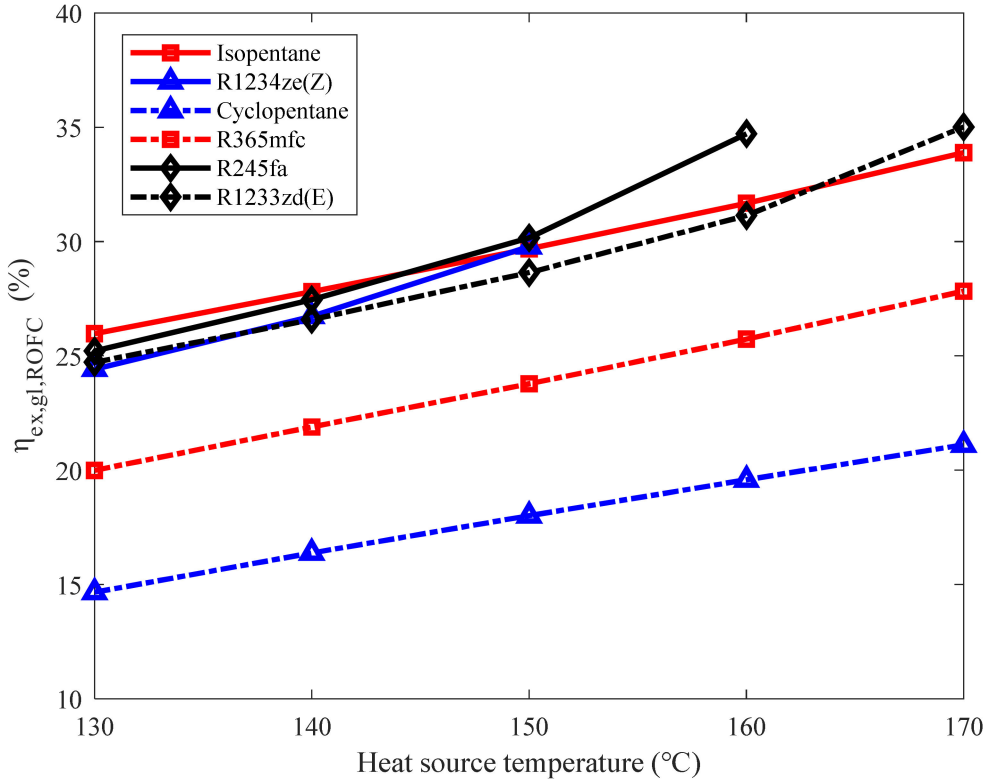


Figure 10. Effect of heat source temperature on global exergy efficiency.

Figure 11 shows the effect of heat source temperature on global thermal efficiency. For all working fluids, the global thermal efficiency increased with an increase in the heat source temperature. The global thermal efficiency for each working fluid increased by around 2.5% as the heat source temperature increased from 130 °C to 170 °C. Notably, the global thermal efficiency for only R245fa increased nonlinearly as the heat source temperature increased, due to a sudden rapid increase in net power output for R245fa, as shown in Figure 9. The maximum global thermal efficiency was achieved when using isopentane, followed by using R245fa, R1233zd(E), R1234ze(Z), R365mfc, and cyclopentane as the working fluid, until a heat source temperature of 140 °C. However, at the heat source temperature of 150 °C, R245fa presented similar a global thermal efficiency to isopentane, and an apparent 0.5% improvement was shown at the heat source temperature of 160 °C. It was also noted that R1233zd(E) was the most superior working fluid, with the highest global thermal efficiency of 6.8%.

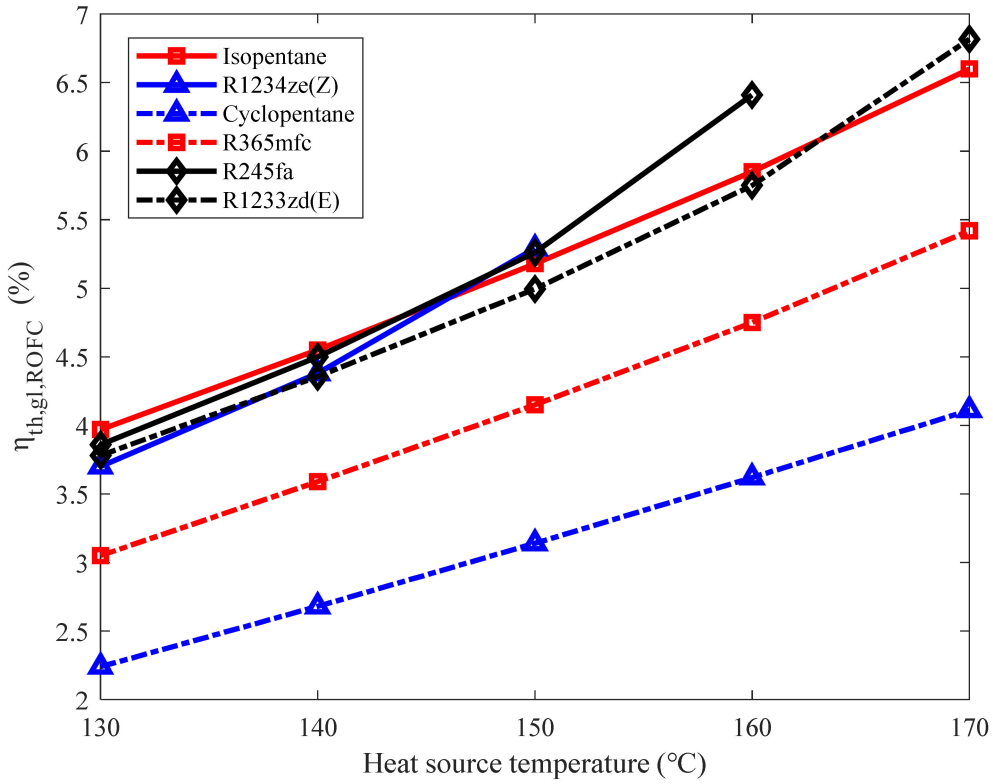


Figure 11. Effect of heat source temperature on global thermal efficiency.

3.4. The Effect of Cooling Water Temperature on ROFC Performance

This section outlines the investigated effect of cooling water temperature on net power output, global exergy efficiency, and global thermal efficiency. Using the control variate method (apart from cooling water temperature, the other parameters were not changed, as indicated in Table 3), the ROFC performance was evaluated for several working fluids.

Figure 12 demonstrates the influence of cooling water temperature on the net power output. As expected, the net power decreased with the coolong water temperature. Working fluid R245fa with the ROFC showed more net power output at cooling water temperatures of 20 °C, 25 °C, and 30 °C, compared to other working fluids. However, at cooling water temperatures of 30–40 °C, R365mfc performed the best among the working fluids.

Figure 13 shows that the global exergy efficiency decreased linearly when the cooling water temperature decreased for all working fluids, due to the reduction in pressure drop through the turbine (the increasing condensation pressure along with the increasing condensation temperature). Therefore, the maximum global exergy efficiency was obtained at a cooling temperature of 20 °C for R245fa as the working fluid. However, the line for isopentane almost covers the line for R245fa. Thus, isopentane also performed better than the other working fluids when the cooling water temperature was less than 30 °C. R365mfc outperformed the selected working fluids at 30–40 °C, with the highest global exergy efficiency.

Figure 14 illustrates the effect of cooling water temperature on the global thermal efficiency. The observed variation trend in global thermal efficiency was similar to the net power output, owing to the same heat input that corresponded to each cooling water temperature. Therefore, the maximum global thermal efficiency for each working fluid occurred at a cooling temperature of 20 °C, and 5.26% was the largest such efficiency for R245fa, compared with R1234ze(Z) and isopentane. At a cooling temperature of 40 °C, the global thermal efficiency of the ROFC was in a similar range for R365mfc, isopentane, R245fa, cyclopentane, R1234ze(Z), and R1233zd(E).

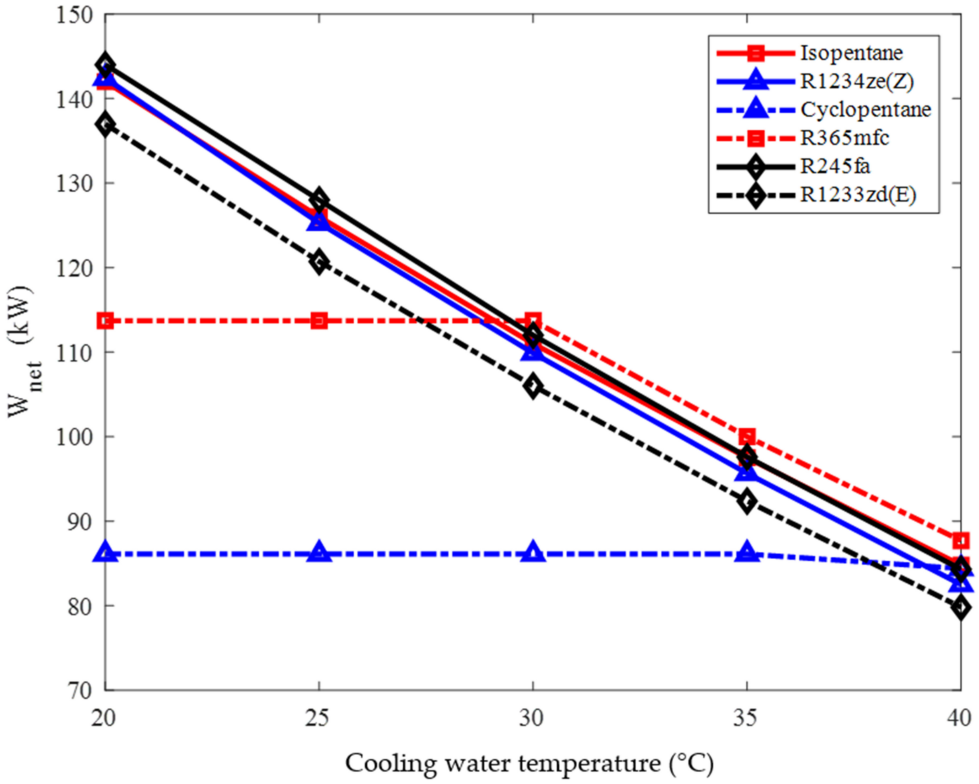


Figure 12. Effect of the cooling water temperature on the net power output.

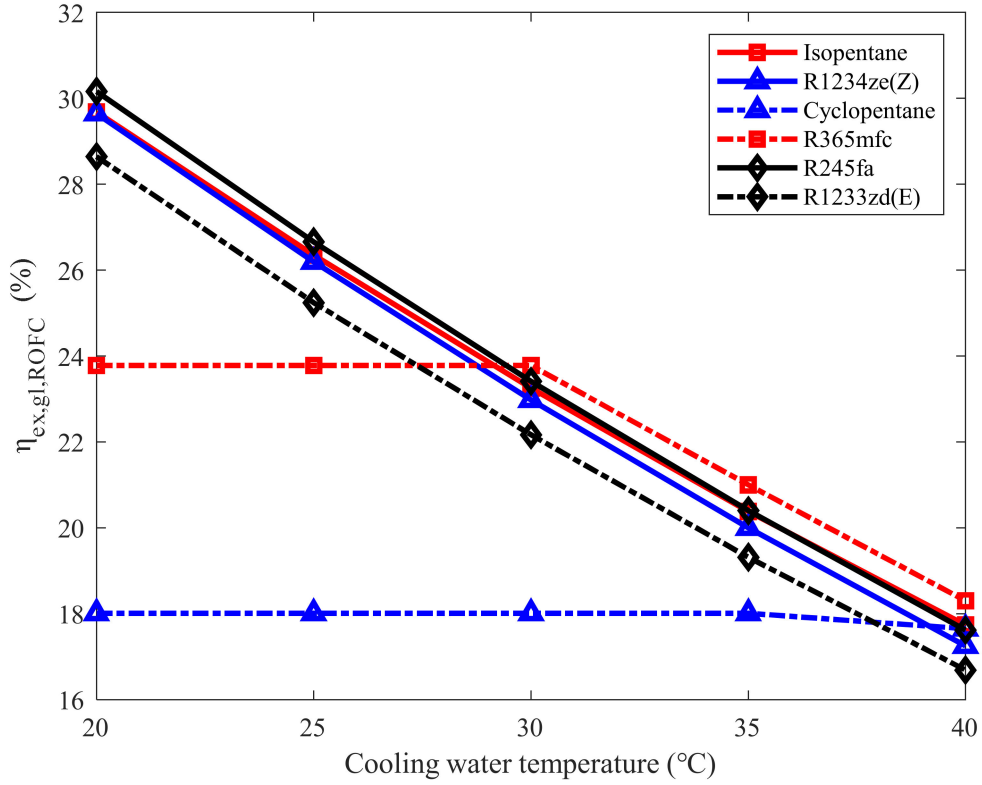


Figure 13. Effect of the cooling water temperature on the global exergy efficiency.

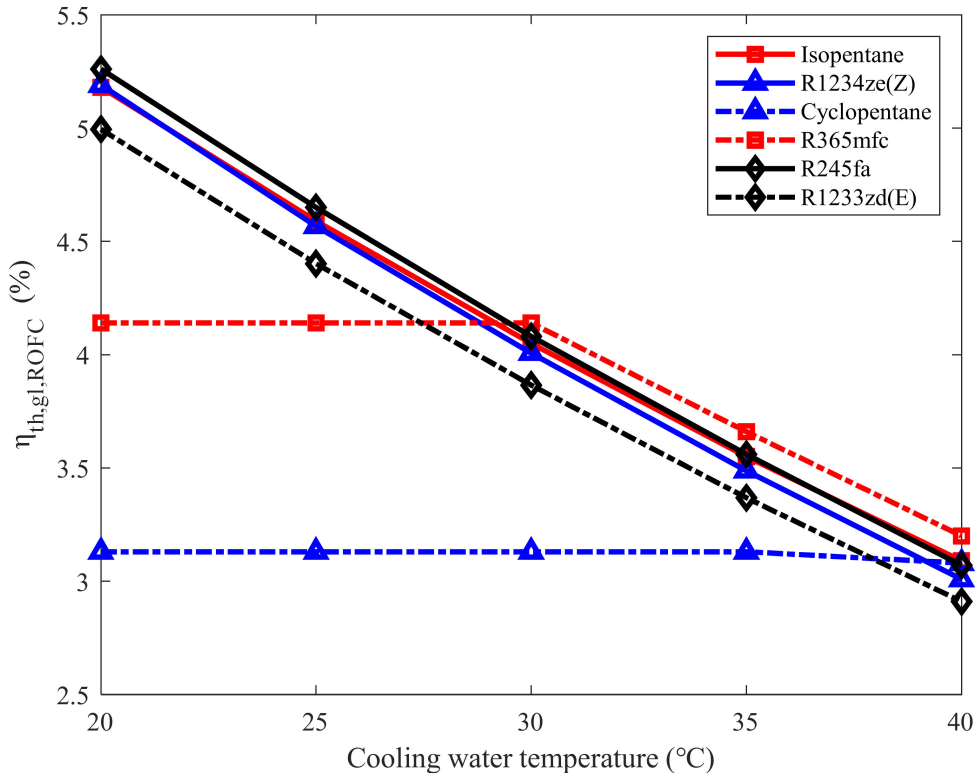


Figure 14. Effect of the cooling water temperature on the global thermal efficiency.

3.5. The Performance of the CHP System Using Isopentane as the Working Fluid throughout a Year

In order to increase thermal efficiency, the ROFC with an optimal working fluid coupled with a WHS was investigated. Table 3 lists the basic conditions required for the thermodynamic analyses; the mass flow rate of the HTF was set as 3 kg/s, in order to match the heating power requirement for the WHS. Considering the thermal efficiency, net power output, exergy efficiency, global exergy efficiency, and exergy destruction, the effect of the monthly heat demand on the CHP system's performance with isopentane as the working fluid was examined.

Figure 15 presents the thermal efficiency and heat transfer demand by month; both showed similar behavior. As depicted in Figure 15, the thermal efficiency and heat transfer demand showed a minimum in August (summer), an increase from September, a maximum in Feburuary, a decrease again from March, with both reaching a minimum in August. The maximum and minimum values of the thermal efficiency and heat transfer demand in August and Feburary were 74.3% and 1160 kW, and 32.8% and 369 kW, respectively. The heat demand for the WHS in the summer was less than that in the winter; thus, the thermal efficiency of the CHP system in the winter was higher than that in other seasons, especially compared to the summer.

Figure 16 shows the monthly net power output that was generated by the CHP system, and the monthly evaporator mass flow rate in mixer1. The monthly behaviour of both quantities (net power output and evaporator mass flow rate) showed a similar trend, since the net power output and turbine mass flow rate were proportional (the larger the mass flow rate, the larger the power output). Notably, the net power output (85 kW) and the mass flow rate (4.56 kg/s) at the inlet of the turbine in July were the same as they were in August, because all of the heat transfer fluid passed through the turbine, and then provided heat to the WHS in July and August. Thus, the heat transfer rate to the ROFC in those two months was more than that in other months. However, most of the heat transfer fluid separated into the mixer in February, where it mixed with a fraction of heat transfer fluid from the evaporator, and flowed through the WHS for the largest heat demand in February; thus, the net power output (37.2 kW) that was generated by the turbine was much lower in February.

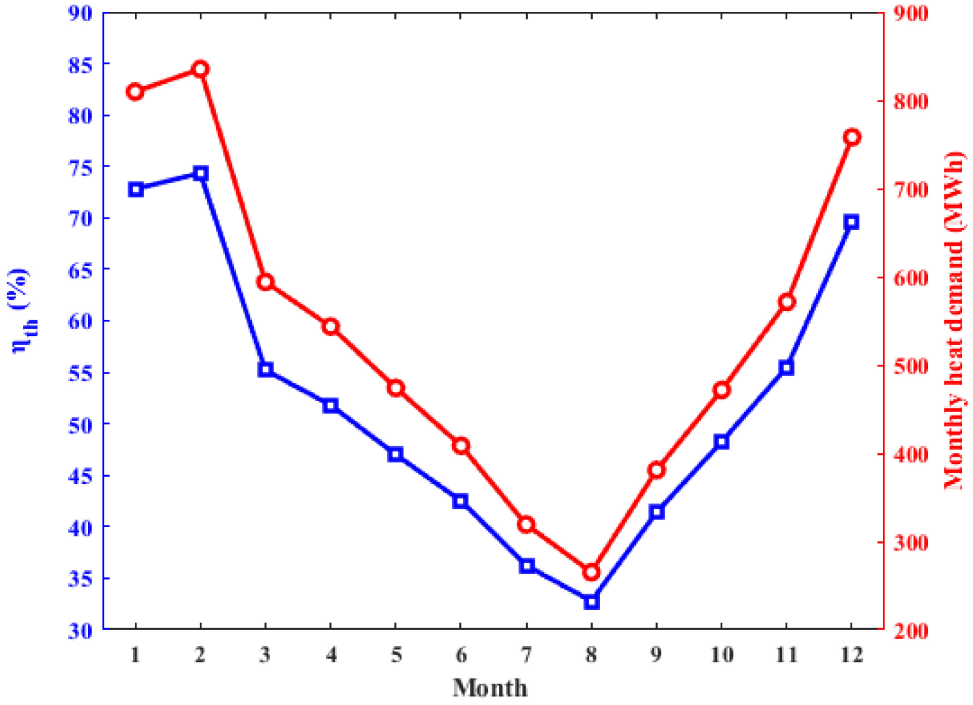


Figure 15. Monthly heat demand and thermal efficiency of the CHP system.

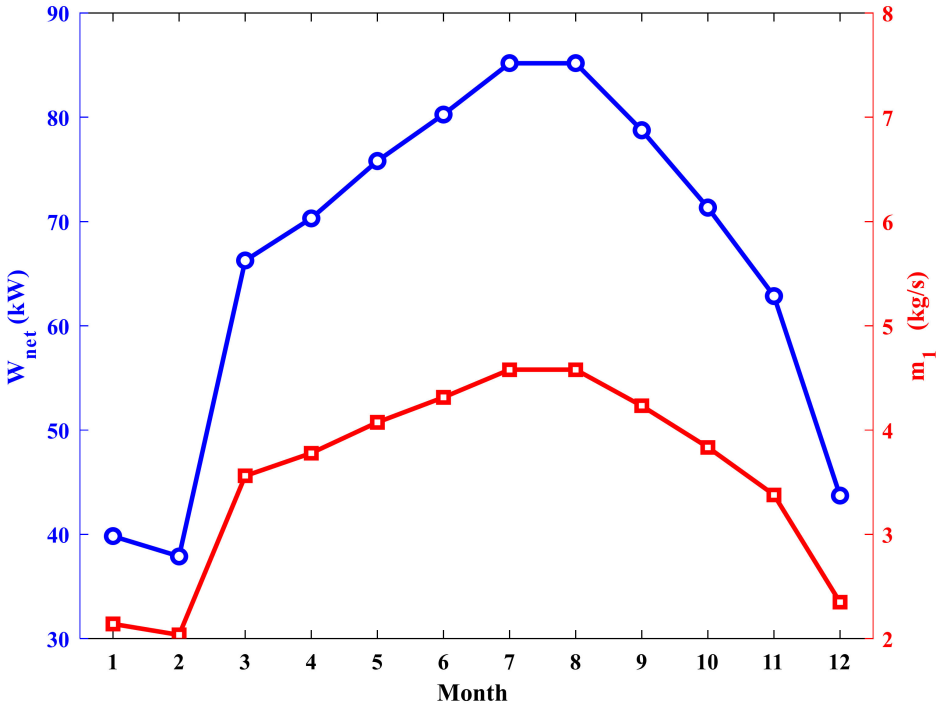


Figure 16. Monthly net power output of the CHP system, and the monthly evaporator mass flow rate in mixer1.

Figure 17 shows the monthly global exergy efficiency and exergy efficiency of the CHP system. The exergy efficiency was higher than the global exergy efficiency for every month of the year. The reason for this is because the global exergy input is always greater than the exergy input when the waste heat temperature at the heat exchanger outlet is equal to the ambient temperature. It can be noted that both global exergy and exergy efficiencies in the summer months were higher than those in the cold months, because more heat transfer fluid flowed through the evaporator to produce power in the summer months, when the heat demand was low.

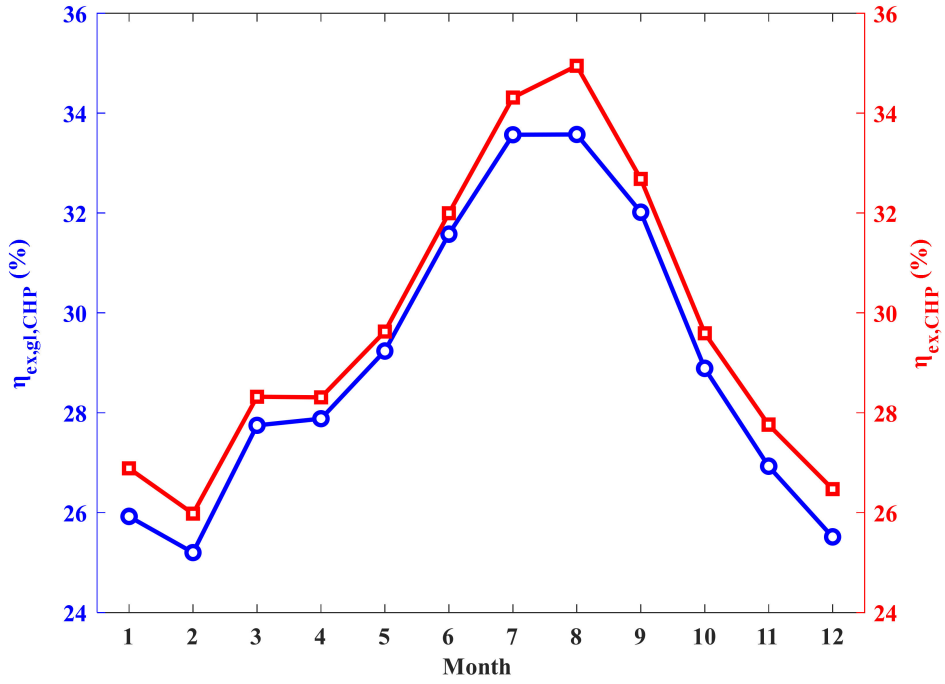


Figure 17. Monthly global exergy efficiency and exergy efficiency of the CHP system.

Figure 18 describes the monthly exergy destruction of each component throughout the year; it can be observed that the global exergy loss in the summer was less than that in the winter. The WHS showed the largest exergy destruction change throughout the year, with a maximum value of 164 kW reached in February, and a minimum value of 36 kW measured in August. The reason for this is because a larger irreversibility in the WHS exists when a larger heat demand must be met in colder months. It can be also observed that the variation in exergy loss in all components of the ROFC was the opposite to that in the WHS and m2, since the increase in heat transfer demand in the WHS decreased the evaporator mass flow.

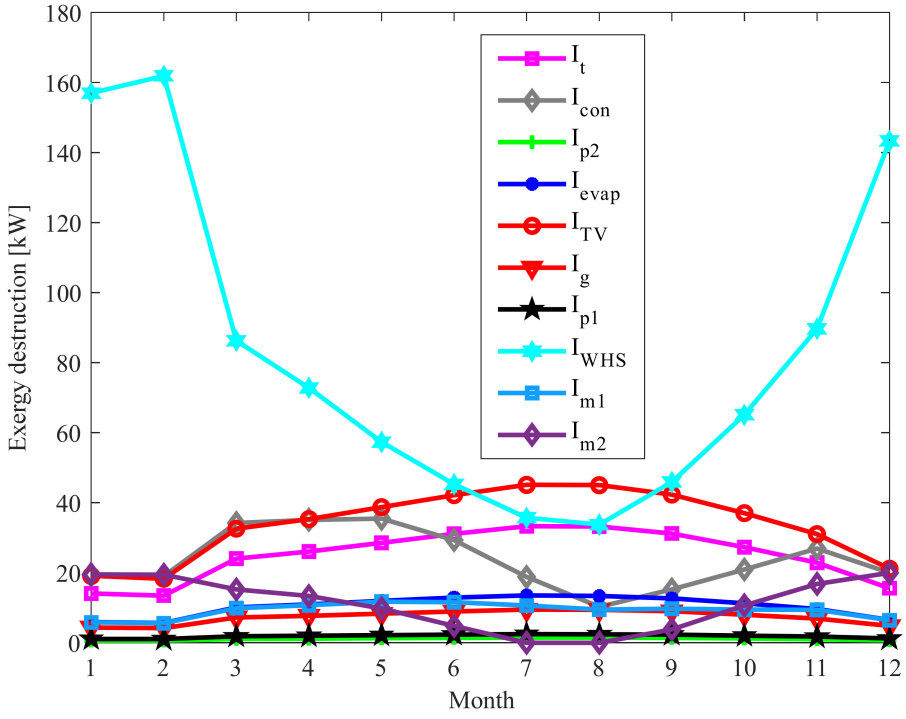


Figure 18. Monthly exergy destruction of each component.

4. Conclusions

In this study, the optimal working fluid for the ROFC was determined, and the monthly performance of the ROFC-based CHP system was investigated using the selected working fluid. According to the energy and exergy analyses, the main conclusions are summarized as follows:

- For each working fluid, the flash pressure affected the ROFC's performance. The net power output increased, and then decreased rapidly as the flash pressure increased; the best net power output was obtained at an optimal flash pressure.
- The results regarding the quantitative analysis of the effects of a heat source and cooling water temperature on the ROFC's performance revealed that the ROFC performed better as the heat source temperature increased, and as the cooling water temperature declined. Furthermore, with a 10 °C increase in the heat source temperature, the global exergy efficiency increased by around 2.5%. In contrast, with a 10 °C increase in the cooling water temperature, the global exergy efficiency decreased by around 2.5%.
- The optimal working fluid for the ROFC was affected by the heat source and cooling water temperature. At a constant cooling water temperature of 20 °C, isopentane and R245fa were the two best working fluids for the ROFC. R245fa performed better when the heat source temperature was $\geq$ 150 °C and $\leq$ 160 °C. At a constant heat source temperature of 150 °C, R365mfc was superior to the other working fluids for the ROFC, when the cooling water temperature was 30–40 °C.
- The following conclusions were reached, in terms of the proposed CHP system's simulation results throughout a year:
  - In February, exergy destruction mainly occurred at the WHS, accounting for 65.0%. The mixer, condenser and throttling valve accounted for 7.80%, 7.64%, and 7.33%, respectively. A more effective system layout of the ROFC-based CHP system can be investigated to further improve system efficiency in the future.
  - In August, exergy destruction occurred on the throttling valve, WHS, and turbine, accounting for 28.46%, 21.30%, and 20.98%, respectively.
  - Compared to the thermal efficiency of 8.37% of the ROFC, the thermal efficiency of the CHP system improved to 32.80% in August, and greatly improved to 74.34% in February.

This study can be utilized as an important reference for the practical engineering applications of the ROFC-based CHP system, on the basis of an economic analysis. In addition, more effective cycle layout of the ROFC-based CHP system can be investigated, in order to further improve the system's efficiency in the future.

Author Contributions: Conceptualization, H.C.; methodology, H.C.; validation H.C.; formal analysis, H.C.; investigation, H.C.; writing—original draft preparation, H.C.; writing—review and editing, M.-H.K.; supervision, M.-H.K. All authors have read and agreed to the published version of the manuscript.

Funding: This research was partly supported by the Korea Evaluation Institute of Industrial Technology (KEIT) grant, funded by the Korean government (MOTIE) (Project No. 20014863).

Institutional Review Board Statement: Not applicable.

Informed Consent Statement: Not applicable.

Data Availability Statement: Data are contained in within the article.

Conflicts of Interest: The authors declare no conflict of interest.

Nomenclature

C_p	specific heat [kJ/(kg·K)]
e	specific exergy [kJ/kg]
h	specific enthalpy [kJ/kg]
$\dot{I}$	exergy destruction rate [kW]
$\dot{m}$	mass flow rate [kg/s]
P	pressure [kPa]
$\dot{Q}$	heat transfer rate [kW]
s	specific entropy [kJ/kg·K]
T	temperature [°C]
W	power [kW]
η	efficiency [%]
x	quality
Abbreviations	
BOFC	basic organic flash cycle
CHP	combined heat and power
CCHP	combined cooling, heating, and power
GWP	global warming potential
HTF	heat transfer fluid
HTX	external heat exchanger
HE	heat exchanger
IEA	international energy agency
IHE	internal heat exchanger
KC	Kalina cycle
Mtoe	million tonnes of oil equivalent
MOFC	modified organic flash cycle
ORC	organic Rankine cycle
OFC	organic flash cycle
OFCT	organic flash cycle with a two-phase expander
ODP	ozone depletion potential
ROFC	organic flash cycle with a regenerator
SCBC	supercritical carbon dioxide Brayton cycle
ST	split turbine
TFC	trilateral flash cycle
WHS	water heating system
Subscripts	
0, 1, 2, … 18	state points
a, b	state points at the three-direction valve
con	condenser
evap	evaporator
g	generator
gl	global
m1	mixer1
m2	mixer2
p1	pump1
p2	pump2
t	turbine
TV	throttling valve

References

1. Kim, M.-H.; Pettersen, J.; Bullard, C.W. Fundamental process and system design issues in CO_2 vapor compression systems. *Prog. Energy Combust. Sci.* **2004**, *30*, 119–174. [CrossRef]
2. Kim, M.-H.; Lee, S.Y.; Mehendale, S.S.; Webb, R.L. Microchannel Heat Exchanger Design for Evaporator and Condenser Applications. *Adv. Heat Transf.* **2003**, *37*, 297–429.
3. Khatoon, S.; Kim, M.-H. Performance analysis of carbon dioxide based combined power cycle for concentrating solar power. *Energy Convers. Manag.* **2020**, *205*, 112416. [CrossRef]

4. Khatoon, S.; Kim, M.-H. Potential improvement and comparative assessment of supercritical Brayton cycles for arid climate. *Energy Convers. Manag.* **2019**, *200*, 112082. [CrossRef]
5. Sung, T.; Kim, S.; Kim, K.C. Thermoeconomic analysis of a biogas-fueled micro-gas turbine with a bottoming organic Rankine cycle for a sewage sludge and food waste treatment plant in the Republic of Korea. *Appl. Therm. Eng.* **2017**, *127*, 963–974. [CrossRef]
6. Ahmadi, A.; El Haj Assad, D.; Jamali, D.H.; Kumar, R.; Li, Z.; Salameh, T.; Al-Shabi, M.; Ehyaei, M. Applications of geothermal organic Rankine Cycle for electricity production. *J. Clean. Prod.* **2020**, *274*, 122950. [CrossRef]
7. Muhammad, U.; Imran, M.; Lee, D.H.; Park, B.S. Design and experimental investigation of a 1kW organic Rankine cycle system using R245fa as working fluid for low-grade waste heat recovery from steam. *Energy Convers. Manag.* **2015**, *103*, 1089–1100. [CrossRef]
8. Liu, C.; Gao, T. Off-design performance analysis of basic ORC, ORC using zeotropic mixtures and composition-adjustable ORC under optimal control strategy. *Energy* **2019**, *171*, 95–108. [CrossRef]
9. Bianchi, G.; Kennedy, S.; Zaher, O.; Tassou, S.; Miller, J.; Jouhara, H. Numerical modeling of a two-phase twin-screw expander for Trilateral Flash Cycle applications. *Int. J. Refrig.* **2018**, *88*, 248–259. [CrossRef]
10. Wang, L.; Li, H.; Bu, X. Thermo-economic investigation of binary flashing cycle for enhanced geothermal system. *Geothermics* **2021**, *89*, 101951. [CrossRef]
11. Pan, M.; Zhu, Y.; Bian, X.; Liang, Y.; Lu, F.; Ban, Z. Theoretical analysis and comparison on supercritical CO_2 based combined cycles for waste heat recovery of engine. *Energy Convers. Manag.* **2020**, *219*, 113049. [CrossRef]
12. Chen, H.; Goswami, D.Y.; Stefanakos, E.K. A review of thermodynamic cycles and working fluids for the conversion of low-grade heat. *Renew. Sustain. Energy Rev.* **2010**, *14*, 3059–3067. [CrossRef]
13. Li, Y.-R.; Du, M.-T.; Wu, C.-M.; Wu, S.-Y.; Liu, C. Potential of organic Rankine cycle using zeotropic mixtures as working fluids for waste heat recovery. *Energy* **2014**, *77*, 509–519. [CrossRef]
14. Smith, I.K. Development of the Trilateral Flash Cycle System: Part 1: Fundamental Considerations. *Proc. Inst. Mech. Eng. Part A J. Power Energy* **1993**, *207*, 179–194. [CrossRef]
15. DiPippo, R. Ideal thermal efficiency for geothermal binary plants. *Geothermics* **2007**, *36*, 276–285. [CrossRef]
16. Baccioli, A.; Antonelli, M.; Desideri, U. Technical and economic analysis of organic flash regenerative cycles (OFRCs) for low temperature waste heat recovery. *Appl. Energy* **2017**, *199*, 69–87. [CrossRef]
17. Baccioli, A.; Antonelli, M. Organic Flash Cycles: Off-design behavior and control strategies of two different cycle architectures for Waste Heat Recovery applications. *Energy Convers. Manag.* **2018**, *157*, 176–185. [CrossRef]
18. Lee, H.Y.; Park, S.H.; Kim, K.H. Comparative analysis of thermodynamic performance and optimization of organic flash cycle (OFC) and organic Rankine cycle (ORC). *Appl. Therm. Eng.* **2016**, *100*, 680–690. [CrossRef]
19. Wang, Q.; Wu, W.; Li, D.; Wang, J.; He, Z. Thermodynamic analysis and optimization of four organic flash cycle systems for waste heat recovery. *Energy Convers. Manag.* **2020**, *221*, 113171. [CrossRef]
20. Meng, D.; Liu, Q.; Ji, Z. Performance analyses of regenerative organic flash cycles for geothermal power generation. *Energy Convers. Manag.* **2020**, *224*, 113396. [CrossRef]
21. Chen, L.X.; Hu, P.; Sheng, C.C.; Zhang, N.; Xie, M.N.; Wang, F.X. Thermodynamic analysis of three ejector based organic flash cycles for low grade waste heat recovery. *Energy Convers. Manag.* **2019**, *185*, 384–395. [CrossRef]
22. Mondal, S.; De, S. Ejector based organic flash combined power and refrigeration cycle (EBOFCP&RC)—A scheme for low grade waste heat recovery. *Energy* **2017**, *134*, 638–648. [CrossRef]
23. Van Erdeweghe, S.; Van Bael, J.; Laenen, B.; D'haeseleer, W. Optimal combined heat-and-power plant for a low-temperature geothermal source. *Energy* **2018**, *150*, 396–409. [CrossRef]
24. Prando, D.; Renzi, M.; Gasparella, A.; Baratieri, M. Monitoring of the energy performance of a district heating CHP plant based on biomass boiler and ORC generator. *Appl. Therm. Eng.* **2015**, *79*, 98–107. [CrossRef]
25. Liao, G.; Liu, L.; Zhang, F.; Jiaqiang, E.; Chen, J. A novel combined cooling-heating and power (CCHP) system integrated organic Rankine cycle for waste heat recovery of bottom slag in coal-fired plants. *Energy Convers. Manag.* **2019**, *186*, 380–392. [CrossRef]
26. Wang, Q.; Wu, W.; He, Z. Thermodynamic analysis and optimization of a novel organic Rankine cycle-based micro-scale cogeneration system using biomass fuel. *Energy Convers. Manag.* **2019**, *198*, 111803. [CrossRef]
27. Arabkoohsar, A.; Nami, H. Thermodynamic and economic analyses of a hybrid waste-driven CHP–ORC plant with exhaust heat recovery. *Energy Convers. Manag.* **2019**, *187*, 512–522. [CrossRef]
28. Rostamzadeh, H.; Ebadollahi, M.; Ghaebi, H.; Shokri, A. Comparative study of two novel micro-CCHP systems based on organic Rankine cycle and Kalina cycle. *Energy Convers. Manag.* **2019**, *183*, 210–229. [CrossRef]
29. Aghahosseini, S.; Dincer, I. Comparative performance analysis of low-temperature Organic Rankine Cycle (ORC) using pure and zeotropic working fluids. *Appl. Therm. Eng.* **2013**, *54*, 35–42. [CrossRef]
30. Tabrizi, K.M.; Bonalumi, D. Techno-economic performance of the 2-propanol/1-butanol zeotropic mixture and 2-propanol/water azeotropic mixture as a working fluid in Organic Rankine Cycles. *Energy* **2022**, *246*, 123316. [CrossRef]
31. Bahrami, M.; Pourfayaz, F.; Kasaeian, A. Low global warming potential (GWP) working fluids (WFs) for Organic Rankine Cycle (ORC) applications. *Energy Rep.* **2022**, *8*, 2976–2988. [CrossRef]

32. Scharrer, D.; Bazan, P.; Pruckner, M.; German, R. Simulation and analysis of a Carnot Battery consisting of a reversible heat pump/organic Rankine cycle for a domestic application in a community with varying number of houses. *Energy* **2022**, *261*, 125166. [CrossRef]
33. Feili, M.; Rostamzadeh, H.; Ghaebi, H. Thermo-mechanical energy level approach integrated with exergoeconomic optimization for realistic cost evaluation of a novel micro-CCHP system. *Renew. Energy* **2022**, *190*, 630–657. [CrossRef]
34. Peris, B.; Navarro-Esbrí, J.; Molés, F.; Mota-Babiloni, A. Experimental study of an ORC (organic Rankine cycle) for low grade waste heat recovery in a ceramic industry. *Energy* **2015**, *85*, 534–542. [CrossRef]
35. Blondel, Q.; Tauveron, N.; Caney, N.; Voeltzel, N. Experimental Study and Optimization of the Organic Rankine Cycle with Pure NovecTM649 and Zeotropic Mixture NovecTM649/HFE7000 as Working Fluid. *Appl. Sci.* **2019**, *9*, 1865. [CrossRef]
36. Cedar Laker Ventures, Inc. Data of Ambient Temperature in Daegu, Korea n.d. Available online: https://ko.weatherspark.com/y/142569/ (accessed on 17 January 2021).
37. Aziz, F.; Salim, M.S.; Kim, M.-H. Performance analysis of high temperature cascade organic Rankine cycle coupled with water heating system. *Energy* **2019**, *170*, 954–966. [CrossRef]
38. Aziz, F.; Mudasar, R.; Kim, M.-H. Exergetic and heat load optimization of high temperature organic Rankine cycle. *Energy Convers. Manag.* **2018**, *171*, 48–58. [CrossRef]
39. Kim, M.-H. Energy and Exergy Analysis of Solar Organic Rankine Cycle Coupled with Vapor Compression Refrigeration Cycle. *Energies* **2022**, *15*, 5603. [CrossRef]
40. Lemmon, E.W.; Bell, I.H.; Huber, M.L.; McLinden, M.O. NIST Standard Reference Database 23: Reference Fluid Thermodynamic and Transport Properties-REFPROP. Version 10.0. Standard Reference Data Program. National Institute of Standards and Technology: Gaithersburg, MD, USA, 2018.
41. Khatoon, S.; Almefreji, N.M.A.; Kim, M.-H. Thermodynamic Study of a Combined Power and Refrigeration System for Low-Grade Heat Energy Source. *Energies* **2021**, *14*, 410. [CrossRef]
42. Wu, C.; Xu, X.; Li, Q.; Li, X.; Liu, L.; Liu, C. Performance assessment and optimization of a novel geothermal combined cooling and power system integrating an organic flash cycle with an ammonia-water absorption refrigeration cycle. *Energy Convers. Manag.* **2021**, *227*, 113562. [CrossRef]
43. ASHRAE. ANSI/ASHRAE Addendum f to ANSI/ASHRAE. *Standard 34-2019*; ASHRAE: Atlanta, GA, USA, 2019.